

Audio Inpainting in Time-Frequency Domain with Phase-Aware Prior

Peter Balušík and Pavel Rajmic

Abstract—The so-called audio inpainting problem in the time domain refers to estimating missing segments of samples within a signal. Over the years, several methods have been developed for such type of audio inpainting. In contrast to this case, a time-frequency variant of inpainting appeared in the literature, where the challenge is to reconstruct missing spectrogram columns with reliable information. We propose a method to address this time-frequency audio inpainting problem. Our approach is based on the recently introduced phase-aware signal prior that exploits an estimate of the instantaneous frequency. An optimization problem is formulated and solved using the generalized Chambolle–Pock algorithm. The proposed method is evaluated both objectively and subjectively against other time-frequency inpainting methods, specifically a deep-prior neural network and the autoregression-based approach known as Janssen-TF. Our proposed approach surpassed these methods in the objective evaluation as well as in the conducted listening test. Moreover, this outcome is achieved with a substantially reduced computational requirement compared to alternative methods.

Index Terms—Audio inpainting, Chambolle–Pock algorithm, instantaneous frequency, time-frequency, sparsity, spectrogram.

I. INTRODUCTION

AUDIO inpainting is the task of replacing missing (or corrupted) parts of a digital audio recording [1]. Such parts are usually referred to as *unreliable* [2], [3]. In the case of audio inpainting in the time domain, they take the form of randomly missing samples or the form of *gaps*, which is the case when unreliable samples are concentrated in one place. Unreliable samples can originate from transmission errors, a faulty equipment during recording, or data corruption. Several methods exist for the inpainting of such gaps: those based on the sparsity of the time-frequency representation of audio [3]–[9], autoregression-based methods such as [10], [11], similarity-based methods [12], [13] and recent methods employing deep learning [14], [15]. Sparsity-based and autoregression-based methods are usually successful at inpainting of shorter gaps (tens of milliseconds), while deep learning-based methods are often able to fill in larger gaps (hundreds of milliseconds up to several seconds).

The above mentioned methods fall into the category of audio inpainting in the time domain. However, many audio codecs, such as MP3, AAC, CELT, etc., utilize the short-time signal spectra [16]. Hence, the idea of audio inpainting in the time-frequency (TF) domain, or *spectrogram inpainting*, arises. Several deep-learning-based methods [17]–[19] have been proposed for spectrogram inpainting. Recently, a method based on autoregression called Janssen-TF [20] has been shown to

The work was supported by the Czech Science Foundation (GAČR) Project No. 23-07294S. The authors would like to thank O. Mokrý for computing the results of the Janssen-TF method.

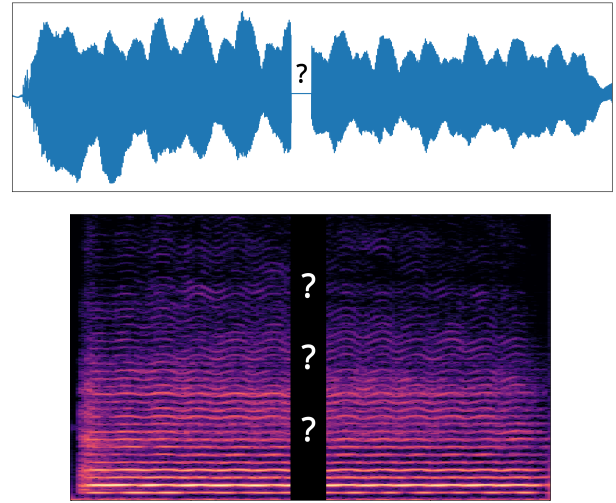


Fig. 1. Audio inpainting problem in the time domain (top) and in the time-frequency domain (bottom).

be the superior method both objectively and subjectively. In the case of spectrogram inpainting, a *gap* refers to missing TF coefficients rather than missing samples. The length of the gap is expressed as the number of missing columns of the spectrogram. Figure 1 illustrates the difference between the gaps in the two domains. Note that the two types of gap are *not equivalent*; see [20], [21].

The spectrogram in Fig. 1 presents a signal representation that is substantially sparser than the signal in the time domain. By sparsity we mean a situation when a vector or matrix consists of a relatively small number of significant elements. For natural signals, suitable transformations can be usually found leading to sparse coefficients. In audio, the short-time Fourier transform (STFT) is often utilized; sparsity-based audio inpainting methods then stem from the observation that the time-frequency coefficients are more or less sparse. The simplest audio inpainting method minimizes the plain sparsity of the spectrogram elements, where the ℓ_1 -norm is often used as a convex approximation, making the problem computationally feasible. More sophisticated methods promote particular structures (mostly horizontal) in the TF representation via a suitable prior.

While inpainting methods based on ℓ_1 -norm minimization have become successful, they come with a number of disadvantages. The main one is the so-called energy loss problem [2], i.e., the amplitude of the reconstructed audio signal decreases towards the center of the gap. This is given by the structure of the STFT and by the inherent properties

of the ℓ_1 -norm. Another problem is the lack of attention to the temporal connections between sinusoidal components in the TF domain [3]. Both of these problems were recently addressed by instantaneous Phase-Corrected Total Variation (iPCTV) prior, originally introduced in [22], and then applied to the time-domain audio inpainting in [23] and [3]. The authors of [3] proposed PHase-aware Audio INpainter (PHAIN) to solve audio inpainting problems in the time domain. One type of their method, known as U-PHAIN, has proven to be the superior method, surpassing even the state-of-the-art Janssen algorithm [10], [24].

This paper integrates the idea of the instantaneous frequency in the problem of inpainting in the time-frequency domain.¹ Therefore, our developed method is abbreviated as U-PHAIN-TF. The proposed method is compared with the Janssen-TF [20] method and the Deep Prior Audio In-painting (DPAI) [19] method, using objective evaluation and a MUSHRA-style listening test. The DPAI method is based on the deep prior approach [25], adapted to inpainting audio instead of images. Even though the method achieved good results, it is highly computationally demanding. The Janssen-TF method has been shown recently to outperform DPAI in terms of both objective and subjective evaluation, while requiring a lower computational effort [20]. We challenge the reconstruction efficiency and computational demand of Janssen-TF with our newly proposed method, U-PHAIN-TF.

The paper is organized as follows. In Section II, the STFT, the problem of spectrogram inpainting, and the generalized Chambolle–Pock algorithm (GCPA) [26] are discussed. Next, in Section III, the concept of phase-aware prior is summarized. The new method, U-PHAIN-TF, is proposed in Section IV. Section V briefly characterizes the reference methods used in the experiments. In Section VI, the proposed method is compared with the reference methods. A thorough discussion of the results is followed by the conclusion in Section VII.

II. PRELIMINARIES

A. Short-time Fourier Transform (STFT)

The discrete-time short-time Fourier transform, also known as the discrete Gabor transform or just STFT, is widely used in time-frequency (TF) signal processing [27]. For a signal $\mathbf{x} \in \mathbb{R}^L$ of length $L \in \mathbb{N}$ and a window function $\mathbf{g} \in \mathbb{R}^L$, the STFT is defined as

$$X[m, n] = (\mathcal{G}_{\mathbf{g}} \mathbf{x})[m, n] = \sum_{l=0}^{L-1} x[l] \cdot g[l - an] \cdot e^{-i2\pi ml/M}, \quad (1)$$

where l indexes the elements of \mathbf{x} , $m \in \{0, 1, \dots, M-1\}$ and $n \in \{0, 1, \dots, N-1\}$ are the frequency and time indices, respectively, and $a \in \mathbb{N}$ is a *hop size* chosen such that $aN = M = L$. Note that the STFT in (1) is an STFT with a frequency-invariant phase [28], [29], and solely this STFT type will be used throughout this paper. In addition, the STFT of the signal \mathbf{x} is indicated by $\mathbf{X} = \mathcal{G}_{\mathbf{g}} \mathbf{x}$, where $\mathbf{X} \in \mathbb{C}^{M \times N}$

¹The concept has been presented as an invited poster at the SampTA 2025 conference; see the abstract at <https://openreview.net/forum?id=j0DHbpebCU>. No actual paper has been published, however.

is a complex *spectrogram*². The entrywise absolute value and the argument can be used to separate the spectrogram into its *magnitude* and *phase* components.

In this paper, exclusively STFT operators satisfying the conditions on the so-called Parseval tight frames will be utilized. They satisfy the following properties [2], [30]

$$\mathcal{G}_{\mathbf{g}}^* \mathcal{G}_{\mathbf{g}} = Id, \quad \|\mathcal{G}_{\mathbf{g}}\|^2 = 1,$$

where Id denotes the identity operator (in this context, the identity on \mathbb{R}^L) and $\mathcal{G}_{\mathbf{g}}^*$ is the adjoint operator of the STFT (often called the inverse STFT) defined as

$$x[l] = (\mathcal{G}_{\mathbf{g}}^* \mathbf{X})[l] = \sum_{m=0}^{M-1} \sum_{n=0}^{N-1} X[m, n] \cdot g[l - an] \cdot e^{i2\pi ml/M}. \quad (2)$$

Note that due to the redundancy of the STFT ($MN > L$), a single spectrogram corresponds to one unique signal, whereas the same signal can be synthesized from multiple spectrograms (depending on the choice of STFT parameters).

B. Sparsity-based Inpainting

As mentioned in Section I, sparsity-based inpainting methods promote particular structures in the TF representation via a suitable prior ϕ , often leading to an optimization problem of the form

$$\operatorname{argmin}_{\mathbf{x} \in \mathbb{R}^L} \phi(\mathcal{G}_{\mathbf{g}} \mathbf{x}) \quad \text{s.t.} \quad \mathbf{x} \in \Gamma_T, \quad (3)$$

where Γ_T is the set of all feasible time-domain signals

$$\Gamma_T = \{\mathbf{x} \in \mathbb{R}^L \mid \mathbf{m} \odot \mathbf{x} = \mathbf{m} \odot \mathbf{x}^{\text{orig}}\}. \quad (4)$$

Here, \mathbf{m} is a binary mask for time signals, indicating unreliable signal samples with zero and reliable elements with one. As an example, the ℓ_1 -norm of a matrix can be used in place of ϕ to obtain a simple time-domain inpainting formulation [2], but more sophisticated priors can be involved [3], [8].

Spectrogram inpainting can be formulated in a similar fashion, presented in the next section.

C. Spectrogram Inpainting

Having the STFT and the spectrogram defined, the actual problem of the time-frequency inpainting can now be formalized. Let us assume that the indices of the gaps, or unreliable parts, are known. For audio inpainting in the time-frequency domain, the following applies:

- $\mathbf{X}^{\text{orig}} \in \mathbb{C}^{M \times N}$ is the ground truth (original) spectrogram obtained as $\mathbf{X}^{\text{orig}} = \mathcal{G}_{\mathbf{g}} \mathbf{x}^{\text{orig}}$, where \mathbf{x}^{orig} is the ground truth signal. Both the ground truth signal and the spectrogram are not known in practice. They are used solely as tools to compute the audio metrics in the objective evaluation (see Section VI-F).
- $\mathbf{M} \in \{0, 1\}^{M \times N}$ is a binary mask analogous to \mathbf{m} , but for spectrograms. As in [18]–[20], the focus is on the case when whole columns of the spectrogram are missing. In

²Note that with \mathbf{x} being real-valued, the spectrogram is symmetric with respect to the frequency axis. Thus, in practice, the frequency dimension can be halved.

such a case, \mathbf{M} comprises of exclusively zero columns or columns of ones.

- $\mathbf{X}^{\text{cor}} \in \mathbb{C}^{M \times N}$ is the observed (corrupted) spectrogram modeled using the binary mask $\mathbf{X}^{\text{cor}} = \mathbf{M} \odot \mathbf{X}^{\text{orig}}$, where \odot is the Hadamard (entrywise) product.
- Consequently Γ_{TF} is the set of all feasible spectrograms

$$\Gamma_{\text{TF}} = \{\mathbf{X} \in \mathbb{C}^{M \times N} \mid \mathbf{M} \odot \mathbf{X} = \mathbf{M} \odot \mathbf{X}^{\text{orig}}\}, \quad (5)$$

i.e., a feasible spectrogram must be consistent with the observation.

- $\iota_{\Gamma_{\text{TF}}}(\mathbf{X})$ is an indicator function of the convex set Γ_{TF} defined as

$$\iota_{\Gamma_{\text{TF}}}(\mathbf{X}) = \begin{cases} 0 & \text{if } \mathbf{X} \in \Gamma_{\text{TF}} \\ \infty & \text{if } \mathbf{X} \notin \Gamma_{\text{TF}} \end{cases}. \quad (6)$$

With this notation, we can write a generic TF-inpainting reconstruction problem as follows:

$$\underset{\mathbf{x} \in \mathbb{R}^L}{\text{argmin}} \phi(\mathcal{G}_{\mathbf{g}} \mathbf{x}) \quad \text{s.t.} \quad \mathcal{G}_{\mathbf{g}} \mathbf{x} \in \Gamma_{\text{TF}}. \quad (7)$$

Note that although the case of entire missing columns of the spectrogram is considered in this paper, generalization to other cases is straightforward.

D. Generalized Chambolle–Pock Algorithm

Proximal algorithms are efficient tools for solving convex minimization problems. The Chambolle–Pock algorithm (CPA), also known as the primal-dual algorithm [26], [31], can be used to solve optimization problems involving one linear operator, such as problem (3), see also [2]. The *generalized* Chambolle–Pock algorithm (GCPA) [26] is an extension of the CPA in two directions: it solves problems involving a linear operator in each of the terms, precisely problems of the form

$$\min_{\mathbf{x}} f(K\mathbf{x}) + g(L\mathbf{x}) + \langle \mathbf{x}, \mathbf{c} \rangle, \quad (8)$$

and the algorithm itself utilizes extrapolation to accelerate convergence. A weak convergence to the solution of the above problem is guaranteed by choosing step sizes $\tau > 0$, $\sigma > 0$, $\eta > 0$ such that $\tau \cdot \sigma \cdot \|L\|^2 \leq 1$ and $\tau \cdot \eta \cdot \|K\|^2 \leq 1$, see [26, Theorem 6.2]).

III. PHASE-AWARE PRIOR

As mentioned, the sparsity of the time-frequency (TF) representation can be enforced via ℓ_1 -based penalties, leading to the energy loss problem [2]. For such penalties, Bayram [32] introduced a simple prior that forces the phase in the spectrogram rows to behave predictably. Although the prior addresses the energy loss problem, it is too simple to provide high-quality solutions. Hence, the instantaneous Phase-Corrected Total Variation (iPCTV) [22] was created. This penalty function is a basic building block of phase-aware audio inpainting methods, such as PHAIN [3], [23], and our proposed method. The iPCTV is defined in the TF domain and it stems from the observation that a pure sinusoid has a predictable phase in the spectrogram. The instantaneous frequency (IF) is estimated at each coefficient of the spectrogram, adapting the penalty to the actual signal content. The iPCTV can be divided into two parts: the instantaneous phase-correction (iPC) part and the total variation (TV) part.

A. Phase Correction

Let $x[l] = e^{i2\pi(\mu+\delta)l/M}$ be a complex exponential where $\delta \in \mathbb{R}$ stands for a frequency shift from the center frequency of the frequency bin $\mu \in \{0, 1, \dots, M-1\}$. It can be shown that the following neighborhood relation holds for the STFT from (1):

$$(\mathcal{G}_{\mathbf{g}} \mathbf{x})[m, n+1] = e^{i2\pi(\mu+\delta-m)a/M} \cdot (\mathcal{G}_{\mathbf{g}} \mathbf{x})[m, n]. \quad (9)$$

The phase values in the μ -th frequency bin can be corrected/compensated by a rotation factor inverse to $e^{i2\pi(\mu+\delta-m)a/M}$, if δ is known [3]. In practice, the relative instantaneous frequency δ of a signal \mathbf{x} is estimated entrywise through [3], [33]

$$\omega_{\mathbf{x}}[m, n] = -\Im \left[\frac{(\mathcal{G}_{\mathbf{g}'} \mathbf{x})[m, n]}{(\mathcal{G}_{\mathbf{g}} \mathbf{x})[m, n]} \right], \quad (10)$$

where \mathbf{g}' is the time-direction derivative of the window \mathbf{g} . Together, these considerations lead to the following phase correction operator on the spectrogram $\mathbf{X} \in \mathbb{C}^{M \times N}$:

$$(\mathcal{R}_{\omega_{\mathbf{x}}} \mathbf{X})[m, n] = e^{-i2\pi a \sum_{t=0}^{n-1} \omega_{\mathbf{x}}[m, t]/M} X[m, n]. \quad (11)$$

Combining such an entrywise operation with the STFT yields a linear transform called instantaneous phase-corrected STFT, which is defined for any signal \mathbf{x} as $\mathcal{R}_{\omega_{\mathbf{x}}} \mathcal{G}_{\mathbf{g}} \mathbf{x}$ [3]. Note that the IF employed in this transform does not need to be calculated directly from \mathbf{x} , which can be exploited depending on the application.

B. Total Variation

In an ideal case of the single sinusoidal \mathbf{x} , the TF coefficients of $\mathcal{R}_{\omega_{\mathbf{x}}} \mathcal{G}_{\mathbf{g}} \mathbf{x}$ are constant over time. In other words, the temporal variation of the phase-corrected STFT is zero across all frequency bins. Formally, the time-directional variation operator $\mathcal{D} : \mathbb{C}^{M \times N} \rightarrow \mathbb{C}^{M \times (N-1)}$ defined as [3]

$$(\mathcal{D} \mathbf{X})[m, n] = X[m, n] - X[m, n+1], \quad (12)$$

where $\mathbf{X} \in \mathbb{C}^{M \times N}$ is a (phase-corrected) spectrogram, yields a zero matrix. The temporal total variation of the spectrogram \mathbf{X} is defined using the ℓ_1 -norm as $\|\mathcal{D} \mathbf{X}\|_1$ [32].

C. Penalty Function: iPCTV

The iPCTV penalty $\|\mathcal{D} \mathcal{R}_{\omega} \mathcal{G}_{\mathbf{g}} \mathbf{x}\|_1$ is a combination of the aforementioned. By minimizing it, sinusoidal components are retained, while components whose phase evolution cannot be approximated by linear functions (such as random noise) are eliminated [3].

D. U-PHAIN for Time-domain Inpainting

Phase correction strongly relies on the instantaneous frequency (IF) estimate. For the basic PHAIN (B-PHAIN) [3], the IF is calculated from the corrupted signal \mathbf{x}^{cor} prior to solving the optimization task, typically resulting in a suboptimal phase correction. This problem is addressed by the novel type of PHAIN, abbreviated U-PHAIN, which introduces a regular instantaneous frequency update [3].

The algorithm of U-PHAIN can be divided into an outer and an inner part. The inner part solves the optimization problem [3]

$$\operatorname{argmin}_{\mathbf{x} \in \mathbb{R}^L} \lambda \|\mathcal{D}\mathcal{R}_\omega \mathcal{G}_g \mathbf{x}\|_1 + \iota_{\Gamma_T}(\mathbf{x}) \quad (13)$$

corresponding to B-PHAIN, where Γ_T is the set of all feasible signals defined in (4) and $\lambda > 0$ is a hyperparameter that adjusts the behavior of the optimization algorithm. Note that g and ω are fixed, and thus the above problem is convex [3]. Problem (13) can be solved using the Chambolle–Pock algorithm (CPA), the same as (3). The outer part updates the IF ω from the temporary solution obtained after each optimization with the CPA.

IV. PHASE-AWARE SPECTROGRAM INPAINTING

With the iPCTV penalty function defined, let us take the problem (8) and make the following substitution:

$$f = \iota_{\Gamma_{\text{TF}}}, \quad g = \lambda \|\cdot\|_1, \quad K = \mathcal{G}_g, \quad L = \mathcal{D}\mathcal{R}_\omega \mathcal{G}_g.$$

Note that the STFT operator is a map $\mathcal{G}_g : \mathbb{R}^L \rightarrow \mathbb{C}^{M \times N}$ and the iPCTV operator is a map $\mathcal{D}\mathcal{R}_\omega \mathcal{G}_g : \mathbb{R}^L \rightarrow \mathbb{C}^{M \times (N-1)}$. In addition, assuming that $\mathbf{c} = \mathbf{0}$, we obtain the following optimization problem for spectrogram inpainting:

$$\operatorname{argmin}_{\mathbf{x} \in \mathbb{R}^L} \lambda \|\mathcal{D}\mathcal{R}_\omega \mathcal{G}_g \mathbf{x}\|_1 + \iota_{\Gamma_{\text{TF}}}(\mathcal{G}_g \mathbf{x}), \quad (14)$$

where Γ_{TF} is the set of all feasible spectrograms defined the same as in (5) and $\lambda > 0$ is a hyperparameter as in (13). This problem is convex when the window g and the instantaneous frequency ω are fixed. In such cases, it can be solved using the generalized Chambolle–Pock algorithm (GCPA) (see Section II-D). Note that to solve it, we need to find the proximal operators of the conjugate functions f^* and g^* , i.e., $\operatorname{prox}_{\eta f^*}$ and $\operatorname{prox}_{\sigma g^*}$; see [26]. The proximal operator of a convex conjugate function $\operatorname{prox}_{f^*}$ can be computed at the same cost as prox_f due to the Moreau identity [2], [34]

$$\operatorname{prox}_{\eta f^*}(\mathbf{x}) = \mathbf{x} - \eta \cdot \operatorname{prox}_{(f/\eta)}(\mathbf{x}/\eta), \quad (15)$$

where $\eta > 0$. In our case, we apply the Moreau identity to yield

$$\operatorname{prox}_{\eta \iota_{\Gamma_{\text{TF}}}^*}(\mathbf{X}) = \mathbf{X} - \eta \cdot \operatorname{proj}_{\Gamma_{\text{TF}}}(\mathbf{X}/\eta), \quad (16)$$

where \mathbf{X} is a spectrogram and $\operatorname{proj}_{\Gamma_{\text{TF}}}$ is the projection onto the convex set Γ_{TF}

$$\operatorname{proj}_{\Gamma_{\text{TF}}}(\mathbf{X}) = \mathbf{M} \odot \mathbf{X}^{\text{cor}} + (1 - \mathbf{M}) \odot \mathbf{X}, \quad (17)$$

which inserts reliable TF coefficients into the input spectrogram, while keeping the unreliable coefficients unchanged [2]. The proximal operator of g^* is defined as

$$\operatorname{prox}_{\sigma(\lambda \|\cdot\|_1)^*}(\mathbf{X}) = \mathbf{X} - \sigma \cdot \operatorname{soft}_{(\lambda/\sigma)}(\mathbf{X}/\sigma) \quad (18)$$

$$= \mathbf{X} - \operatorname{soft}_\lambda(\mathbf{X}), \quad (19)$$

where $\operatorname{soft}_\lambda$ is the soft thresholding operator

$$\operatorname{soft}_\lambda(\mathbf{X}) = \operatorname{sgn}(\mathbf{X}) \odot \max(|\mathbf{X}| - \lambda, 0), \quad (20)$$

where $\operatorname{sgn}(\cdot)$ is the sign function.

The proposed method is called an instantaneous-frequency-Update PHase-aware Audio INpainter in the Time-Frequency domain (U-PHAIN-TF). It minimizes iPCTV, thereby addressing the energy loss problem. Moreover, it promotes the time continuity of the sinusoidal TF coefficients. The method is summarized in Alg. 1. Its inner loop ($i = 1, \dots, I$) uses GCPA

Algorithm 1: U-PHAIN-TF: using GCPA to solve the minimization problem (14).

```

1 Input a peak-normalized corrupted spectrogram  $\mathbf{X}^{\text{cor}}$ .
2 Choose  $\tau, \sigma, \eta > 0$  such that  $\tau \cdot \sigma \cdot \|\mathcal{D}\mathcal{R}_\omega \mathcal{G}_g\|^2 \leq 1$  and
    $\tau \cdot \eta \cdot \|\mathcal{G}_g\|^2 \leq 1$ ;  $\alpha = 1$ .
3 Initialize variables  $\mathbf{x}^{(0)} = \mathcal{G}_g^* \mathbf{X}^{\text{cor}}$ ,  $\mathbf{Y}^{(0)} = \mathbf{0}$ , and  $\mathbf{Z}^{(0)} = \mathbf{0}$ .
4 Set output variable  $\hat{\mathbf{x}}^{(0)} = \mathbf{x}^{(0)}$ ; set  $I, J$ , and threshold  $\varepsilon > 0$ .
5 for  $j = 0, \dots, J$  do
6    $\omega^{(j)} = -\Im[\mathcal{G}_g' \hat{\mathbf{x}}^{(j)} \oslash \mathcal{G}_g \hat{\mathbf{x}}^{(j)}]$ 
7   for  $i = 0, \dots, I$  do
8      $\mathbf{R} = \mathbf{Y}^{(i)} + \eta \cdot \mathcal{G}_g(\mathbf{x}^{(i)} - \tau \cdot (\mathcal{G}_g^* \mathcal{R}_{\omega^{(j)}}^* \mathcal{D}^* \mathbf{Z}^{(i)} + \mathcal{G}_g^* \mathbf{Y}^{(i)}))$ 
9      $\mathbf{Y}^{(i+\frac{1}{2})} = \mathbf{R} - \eta \cdot \operatorname{proj}_{\Gamma_{\text{TF}}}(\mathbf{R}/\eta)$ 
10     $\mathbf{x}^{(i+\frac{1}{2})} = \mathbf{x}^{(i)} - \tau \cdot (\mathcal{G}_g^* \mathcal{R}_{\omega^{(j)}}^* \mathcal{D}^* \mathbf{Z}^{(i)} + \mathcal{G}_g^* \mathbf{Y}^{(i+\frac{1}{2})})$ 
11     $\mathbf{Q} = \mathbf{Z}^{(i)} + \sigma \cdot \mathcal{D}\mathcal{R}_{\omega^{(j)}} \mathcal{G}_g(2 \cdot \mathbf{x}^{(i+\frac{1}{2})} - \mathbf{x}^{(i)})$ 
12     $\mathbf{Z}^{(i+\frac{1}{2})} = \mathbf{Q} - \operatorname{soft}_\lambda(\mathbf{Q})$ 
13     $\mathbf{x}^{(i+1)} = \mathbf{x}^{(i)} + \alpha^{(i)}(\mathbf{x}^{(i+\frac{1}{2})} - \mathbf{x}^{(i)})$ 
14     $\mathbf{Y}^{(i+1)} = \mathbf{Y}^{(i)} + \alpha^{(i)}(\mathbf{Y}^{(i+\frac{1}{2})} - \mathbf{Y}^{(i)})$ 
15     $\mathbf{Z}^{(i+1)} = \mathbf{Z}^{(i)} + \alpha^{(i)}(\mathbf{Z}^{(i+\frac{1}{2})} - \mathbf{Z}^{(i)})$ 
16  end
17   $\hat{\mathbf{x}}^{(j+1)} = \mathbf{x}^{(I)}$ 
18  if  $\|\hat{\mathbf{x}}^{(j)} - \hat{\mathbf{x}}^{(j-1)}\|_2 < \varepsilon$  then
19    break
20  end
21 end
22 return  $\operatorname{proj}_{\Gamma_{\text{TF}}}(\mathcal{G}_g \hat{\mathbf{x}})$ 

```

to solve (14). The outer loop ($j = 1, \dots, J$) provides regular instantaneous frequency (IF) update (line 6 of Alg. 1). The symbol \oslash at line 6 denotes the entrywise division.

One primal and two dual variables are introduced in the GCPA, in our case, $\mathbf{x} \in \mathbb{R}^L$, $\mathbf{Y} \in \mathbb{C}^{M \times N}$ and $\mathbf{Z} \in \mathbb{C}^{M \times (N-1)}$. Additionally, during the algorithm, two temporary variables $\mathbf{R} \in \mathbb{C}^{M \times N}$ and $\mathbf{Q} \in \mathbb{C}^{M \times (N-1)}$ are utilized along with a relaxation parameter $\alpha^{(i)} \in (0, 2)$. In particular, we consider the setting $\alpha = 1$, same as in [3]. The desired output of the algorithm is a reconstructed spectrogram $\hat{\mathbf{X}}$.

Note that phase-aware spectrogram inpainting can be formulated in several different ways beyond (14). We have also analyzed a problem formulated solely in the time–frequency domain; see Appendix A. However, such an approach turned out to be less efficient than Alg. 1. The results indicate that it is important when the variables of the GCPA alternate between the time domain and the TF domain. We also examined alternative thresholding operators to soft thresholding and alternative norms to the ℓ_1 -norm; see Appendix B. Nevertheless, soft thresholding performed the best in terms of objective metrics, suggesting that the use of the ℓ_1 -norm is beneficial.

V. REFERENCE METHODS

Several approaches to spectrogram inpainting have recently emerged, including Deep Prior Audio Inpainting (DPAI) [19], and the current state-of-the-art, Janssen-TF [20].

A. Deep Prior Audio Inpainting (DPAI)

DPAI is a deep-prior-based method that uses a convolutional neural network (CNN) whose architecture itself (without external training) acts as the regularizer for audio inpainting. The CNN is then overfitted on a single degraded spectrogram and a solution is obtained by early stopping of the process.

In [19], the authors consider a CNN described by the function $f_\theta(\mathbf{N})$, where θ is a set of trainable network parameters (weights and biases) and $\mathbf{N} \in \mathbb{C}^{M \times N}$ is a random fixed noise matrix. The main assumption is that the CNN can generate any spectrogram $\mathbf{X} \in \mathbb{C}^{M \times N}$ from \mathbf{N} using a suitable θ . Note that θ is initialized randomly and then optimized as

$$\theta^* = \underset{\theta}{\operatorname{argmin}} E(\mathbf{M} \odot f_\theta(\mathbf{N}), \mathbf{X}^{\text{cor}}), \quad (21)$$

where $E(\cdot)$ is a loss function that combines the mean squared error and the multi-scale spectrogram loss [35]. The optimal θ^* is acquired using standard optimizers such as Adam [36]. The reconstructed spectrogram $\hat{\mathbf{X}}$ is obtained by early stopping of the optimization, i.e., before overfitting occurs. Here, overfitting refers to the case where $f_{\theta^*}(\mathbf{N}) = \mathbf{X}^{\text{cor}}$.

B. Janssen-TF

Janssen-TF is a recent adaptation of the Janssen algorithm [10] to the TF case. It is based on autoregressive (AR) modeling. Thus, it utilizes harmonic components of a spectrogram near the gaps to predict the values of missing TF coefficients. It repeats two main steps in the i -th iteration. First, given an estimate of a signal $\mathbf{x}^{(i)}$, compute the parameters of an AR model, which are denoted $\mathbf{a}^{(i)}$. Second, by creating a Toeplitz matrix $\mathbf{A}^{(i)}$ composed of the coefficients $\mathbf{a}^{(i)}$, estimate a new solution $\mathbf{x}^{(i+1)}$ as

$$\mathbf{x}^{(i+1)} = \arg \min_{\mathbf{x}} \frac{1}{2} \|\mathbf{A}\mathbf{x}\|^2 + \iota_{\Gamma_{\text{TF}}}(\mathcal{G}\mathbf{x}), \quad (22)$$

where Γ_{TF} is the set (5). The authors of [20] used the alternating direction method of multipliers (ADMM) to solve the above problem, as it delivered the best performance. However, other proximal algorithms are viable; see [20].

VI. EXPERIMENTS AND RESULTS

A. Datasets

Two datasets were chosen: the dataset used in [19], [20], which will be called the DPAI dataset, and the IRMAS dataset [37].

1) *DPAI dataset*: As mentioned above, DPAI will be utilized in the experiments as one of the reference methods. The authors of DPAI tuned the network architecture and hyperparameters on their proprietary dataset, which is why this dataset will be used in the comparison. The DPAI dataset consists of eight recordings, each 5 seconds long, sampled at 16 kHz.

2) *IRMAS dataset*: The dataset comprises over 6000 audio recordings featuring various musical instruments, including cello, clarinet, flute, guitar, violin, and others, as well as recordings of a singing voice. Due to the large number of recordings, only a subset of IRMAS will be used. The subset³, also used in [20], consists of 60 recordings, each 5 seconds long, sampled at 16 kHz. With its 60 recordings, this dataset can provide more reliable results than the DPAI dataset in the objective comparison.

B. Masks

The same masks as in [20] were chosen for fair comparison. The masks are designed for 5-second spectrograms, containing one gap in each second. The gap length ranges from 1 to 6 missing (zero) columns, 6 masks in total. Figure 2 illustrates three examples.

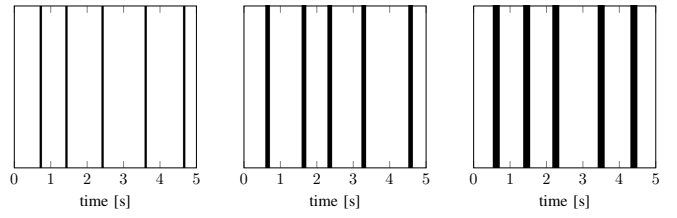


Fig. 2. Different masks used in experiments. Each mask has five gaps with length ranging from 1 missing column to 6 missing columns. Here, only the second mask (left), fourth mask (middle), and sixth mask (right) is shown.

The number of signal samples affected by the spectrogram gaps (zero columns) can be calculated. In our case, the affected regions range from 2048 samples (mask one) to 4608 samples (mask six), i.e., from 128 ms to 288 ms.

C. Metrics

The Signal-to-Noise Ratio (SNR) is a well-known metric, defined in decibels as in [1]:

$$\text{SNR}(\mathbf{x}^{\text{orig}}, \hat{\mathbf{x}}) = 10 \cdot \log_{10} \left(\frac{\|\mathbf{x}^{\text{orig}}\|^2}{\|\mathbf{x}^{\text{orig}} - \hat{\mathbf{x}}\|^2} \right), \quad (23)$$

where $\hat{\mathbf{x}}$ is the reconstructed signal obtained from the reconstructed spectrogram by $\hat{\mathbf{x}} = \mathcal{G}_g^* \hat{\mathbf{X}}$. The Objective Difference Grade (ODG), computed using PEMO-Q v1.4.1 [38], is an estimate of subjective perception of restoration quality. It predicts the quality impairment of the reconstructed signal $\hat{\mathbf{x}}$ relative to the reference (original) signal \mathbf{x}^{orig} on a continuous scale from -4 to 0 : Imperceptible (0); Perceptible but not annoying (-1); Slightly annoying (-2); Annoying (-3); Very annoying (-4).

Some studies evaluate the SNR only within the gap regions [2], [4], [19], [24], whereas other works [3], [20] compute it over the entire signal. In the case of inpainting, assuming that the output of the method is a projection onto the feasible set Γ_T (or Γ_{TF}), it can be shown that the SNR computed on the entire signal (or spectrogram) is the SNR in gaps plus a term

³The list of the recordings used and the code to crop and subsample them can be found at <https://github.com/rajmic/spectrogram-inpainting/tree/main/audio-irmas>.

dependent only on the ground truth. The ODG is computed only on the entire signal. Therefore, in this paper, both SNR and ODG are computed over the *entire* signal.

D. Implementation

The source codes for our proposed method, U-PHAIN-TF, are publicly available at <https://github.com/sedemto/phain-tf>. The proposed method was implemented in Matlab R2025a, drawing mainly on the Matlab codes⁴ from the original U-PHAIN [3]. In addition, we utilized the Large Time-Frequency Analysis Toolbox (LTFAT) [39] for fast computation of time-frequency transformations⁵ needed within U-PHAIN.

Before running the algorithm, the input data (corrupted spectrograms) are divided into smaller spectrogram segments. Peak values are computed from the associated time-domain signals and used to perform peak-normalization of the segments. The need for normalization is justified in Appendix C. Each spectrogram segment contains a single gap and a reliable context around it. The context window is controlled by the hyperparameter `pad`, which specifies the minimum number of spectrogram columns taken from either side of the gap. Initially, `pad` is set equal to the window length over the hop size (L/a), which proved sufficient in our preliminary experiments. The number of columns taken from each side of the gap is then adjusted according to two conditions:

- The STFT implementation in the LTFAT toolbox requires the segment length to be a multiple of L/a (see [39]).
- Since an STFT with frequency-invariant phase is used, the starting index of the segment, minus one, must be divisible by L/a .⁶

Note that both conditions are required to ensure that the method works as intended. From such segments, we calculate the initial value of the primal variable in Alg. 1, i.e., $\mathbf{x}^{(0)}$ in the time domain. The algorithm can now be used to obtain a reconstructed spectrogram segment. In the end, spectrogram segments obtained by Alg. 1 are de-normalized and inserted into the observed corrupted spectrograms.

E. Choice of Hyperparameters

U-PHAIN-TF involves a number of hyperparameters, such as the STFT parameters (window length, window type, hop size, FFT length), the regularization parameter λ , parameters of the GCPA (step sizes σ , η , τ , threshold ε , number of inner I and outer iterations J), and parameter `pad`.

1) *STFT parameters*: For the STFT, we use a 2048-sample-long Hann window (corresponding to 128 ms) with a 75% overlap and 2048 frequency channels, such that \mathcal{G}_g forms a Parseval tight frame. The parameters are the same as in [20]

⁴Matlab codes of U-PHAIN (and others types of PHAIN) are publicly available at <https://doi.org/10.24433/CO.1956970.v1>. In addition, some functions from <https://doi.org/10.24433/CO.2743732.v1> were utilized.

⁵The codes for a faster computation of U-PHAIN are publicly available at <https://github.com/sedemto/phain-ltfat>.

⁶For an STFT with time-invariant phase, as used in [20], this condition can be omitted.

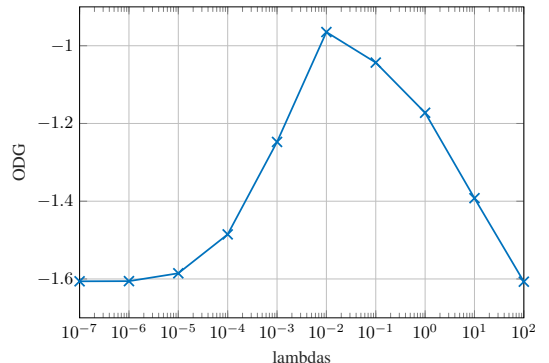


Fig. 3. Objective results for U-PHAIN-TF with different setting of lambda. The ODG results are computed on the DPAI dataset with all masks applied to each example. For each setting of λ , the results are averaged across all examples and masks.

and they were chosen to provide a fair comparison with the reference methods. In addition, we calculate the time-directional derivative of the window (\mathbf{g}' required in (10)) analytically. Alternatively, a spectral derivative may be employed; see [40].

2) *Lambda*: Given that the input data are normalized (see Appendix C), the optimal value of lambda can be determined. We computed the ODG metric on the reconstructions from the DPAI dataset, for lambdas ranging from 10^{-7} to 10^2 . From Fig. 3, it can be seen that the optimal value is about 10^{-2} . Note that the same observation applies if SNR is considered.

3) *Step sizes*: The step sizes for U-PHAIN-TF are chosen such that $\tau \cdot \sigma \cdot \|\mathcal{DR}_\omega \mathcal{G}_g\|^2 \leq 1$ and $\tau \cdot \eta \cdot \|\mathcal{G}_g\|^2 \leq 1$. From Section II-A, it is known that $\|\mathcal{G}_g\|^2 = 1$; thus, $\eta = 4$ and $\tau = 0.25$ to satisfy the upper limit of the condition. In addition, by defining an operator \mathcal{A} that delays any spectrogram along the time axis, the operator norm of \mathcal{DR}_ω is upper-bounded by:

$$\|\mathcal{DR}_\omega\| = \|\mathcal{R}_\omega - \mathcal{A}\mathcal{R}_\omega\| \leq \|\mathcal{R}_\omega\| + \|\mathcal{A}\mathcal{R}_\omega\| = 2. \quad (24)$$

Note that this formulation is possible since both \mathcal{A} and \mathcal{R}_ω are unitary operators [32]. Using the above, the operator norm $\|\mathcal{DR}_\omega \mathcal{G}_g\|^2 = 4$; hence, $\sigma = 1$ and $\tau = 0.25$. Consequently, a weak convergence is guaranteed in each inner loop.

4) *Iterations*: We have also investigated the number of inner (I) and outer iterations (J) in the proposed context of spectrogram inpainting. First, we fixed J to 10 (same as in [3]) and set the stopping threshold $\varepsilon = 0.001$. Then, we computed the metrics on the DPAI dataset while changing I (i.e., the iteration count of the GCPA). The results of this experiment are shown in Fig. 4. We observe that the metrics start to change more slowly at around 500 iterations. Thus, we selected $I = 500$ as it offers high reconstruction quality while saving some computational time. Finally, we examined the parameter J , i.e., the number of instantaneous frequency updates. The experiments shown in Fig. 5 indicate that the setting $J = 10$ is sufficient and that larger values of J yield little or no additional benefit. Moreover, in many cases, the stopping criterion ($\|\hat{\mathbf{x}}^{(j)} - \hat{\mathbf{x}}^{(j-1)}\|_2 < \varepsilon$) was even met before reaching $J = 10$.

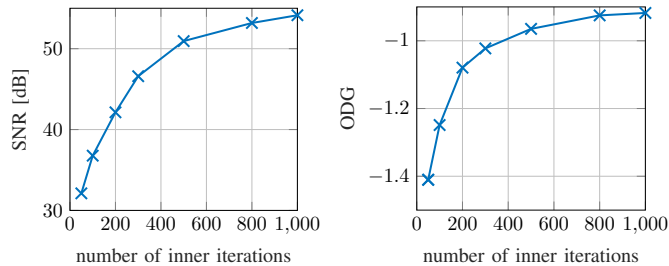


Fig. 4. Results from U-PHAIN-TF with different settings of inner iterations, while the number of outer iterations was fixed to $J = 10$. The SNR (left) and ODG (right) are computed on the DPAI dataset and averaged across all examples and masks.

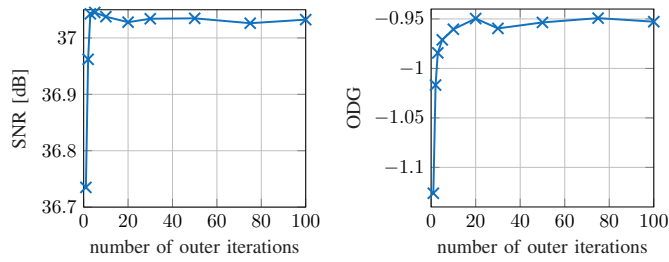


Fig. 5. Results from U-PHAIN-TF with different settings of outer iterations, while the number of inner iterations was fixed to $I = 500$. The SNR (left) and ODG (right) are computed on the DPAI dataset and averaged across all examples and masks.

F. Objective Evaluation

This section compares the proposed method with other TF-domain inpainting methods, specifically Deep Prior Audio Inpainting (DPAI) [19] and Janssen-TF [20] briefly described in Sec. V. For DPAI, the “DPAI with context” variant using the “best2” architecture is employed, which is its strongest-performing configuration in [20]. The execution time is also measured for all methods. The results are averaged over all the examples in each dataset for every mask (see Section VI-B). In the figures that will follow, the horizontal axis represents the masks as “gap length”, while the vertical axis represents the corresponding objective metric (ODG or SNR).

1) *Results on DPAI dataset:* The objective metrics computed on the DPAI dataset are shown in Fig. 6. The bold lines in the middle represent the mean values. The surrounding intervals indicate their values at the 5% significance level. Because the DPAI dataset contains only eight examples, these confidence intervals are relatively wide. Nonetheless, U-PHAIN-TF achieves the best performance in terms of ODG among the compared inpainting methods. As for the SNR, it attains results comparable (large gaps) or greater (short gaps) to those of Janssen-TF. Thus, optimization with the iPCTV appears to have aided in the reconstruction quality.

2) *Results on IRMAS dataset:* The objective metrics computed on the subset of the IRMAS dataset are shown in Fig. 7. In terms of ODG, U-PHAIN-TF clearly surpasses all other inpainting methods. Moreover, the confidence interval of U-PHAIN-TF is outside of the intervals of DPAI and Janssen-TF, making their differences statistically significant. The SNR results are similar to those computed on the DPAI dataset. That is, U-PHAIN-TF outperforms Janssen-TF for

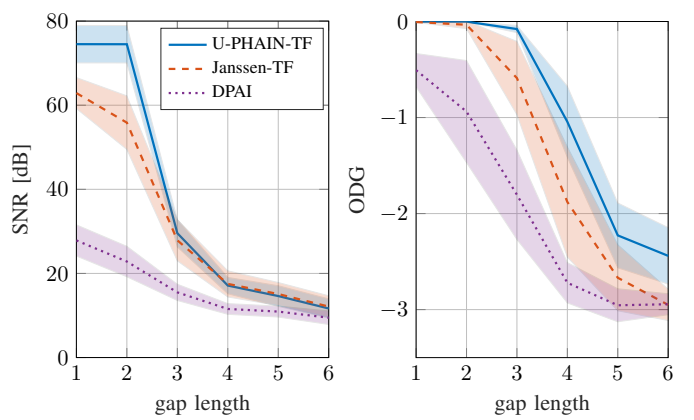


Fig. 6. Comparison on the DPAI dataset of the proposed method with other TF domain inpainting methods in terms of mean SNR (left) and ODG (right). The interval shows estimates of the mean values at the 5% significance level. Wherever the intervals do not overlap, it may be concluded that the difference of the means is statistically significant.

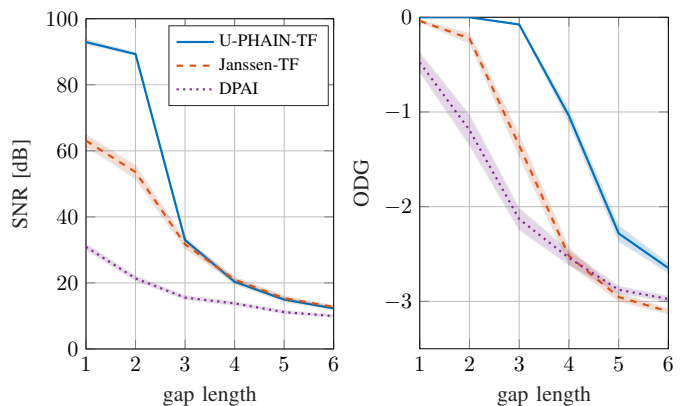


Fig. 7. Comparison on the IRMAS dataset of the proposed method with other TF domain inpainting methods in terms of mean SNR (left) and ODG (right).

smaller gap lengths. For larger gap lengths, U-PHAIN-TF and Janssen-TF achieve comparable SNR results.

Figure 8 shows additional scatter plots that compare the objective scores of Janssen-TF with those of U-PHAIN-TF in more detail. The SNR values show that for larger gaps, the methods perform similarly, confirming the previous cumulative findings. However, the ODG results are strongly biased towards U-PHAIN-TF.

3) *Execution time:* Authors of [20] report that reconstructing a 5-second spectrogram with 5 gaps using the DPAI method takes approximately 19 minutes on an NVIDIA Tesla V100S GPU with 32 GB of memory, regardless of the gap length. We tested the same reconstruction with Janssen-TF and our proposed method (in Matlab R2025a). The computational cost of both methods increases with the gap length. The results of this experiment are summarized in Table I. The execution time of U-PHAIN-TF is shown to be by far the lowest among the methods: it is about 6–42 seconds.

G. Subjective Evaluation

To confirm the objective comparison, a listening test was performed using the MUSHRA method [41]. Six examples

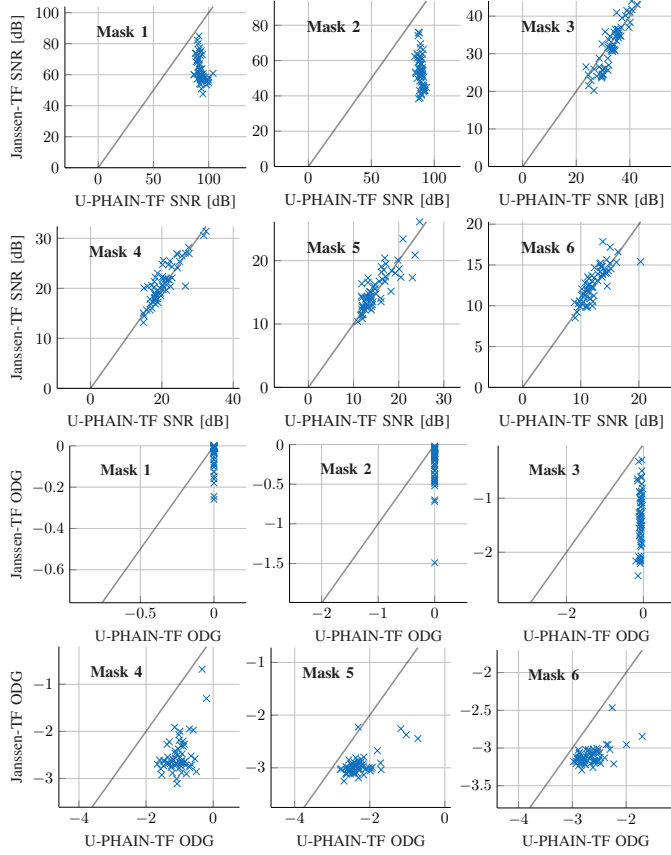


Fig. 8. Scatter plots comparing SNR and ODG scores of Janssen-TF and U-PHAIN-TF for each mask (1–6 missing spectrogram columns). The gray line indicates identical performance.

TABLE I
COMPUTATIONAL DEMAND OF DIFFERENT INPAINTING METHODS.

Method	CPU/GPU	Time (min)
DPAI	NVIDIA Tesla V100S, 32 GB	19
Janssen-TF	AMD Ryzen 9 9900X, 4.4 GHz	5–9
U-PHAIN-TF	AMD Ryzen 9 9900X, 4.4 GHz	0.1–0.7

from the DPAI dataset (0, 1, 3, 4, 5, and 7) were selected, while examples 2 and 6 were omitted for being overly atypical. Furthermore, only three gap lengths (2, 4, and 6) were chosen. The proposed U-PHAIN-TF was evaluated against DPAI and Janssen-TF in this listening test.

For the test, the webMUSHRA environment was utilized [42]. There were five conditions in total: a hidden reference signal, an anchor signal (the corrupted signal computed from the corrupted spectrogram) and three reconstructions corresponding to each of the inpainting methods. With six examples and three masks, the entire test consisted of 18 test pages. Participants rated how similar each signal was to the reference on a continuous scale from 0 to 100. The test took place in a quiet music studio with a professional sound card and headphones. The listening conditions were identical for all participants. In line with [41], 17 of the 21 assessors were retained after post-screening.

The results for each method are depicted using a box plot in Fig. 9. The median score of U-PHAIN-TF is the highest among

all methods, indicating that it is the most promising method for inpainting in the time-frequency domain. Moreover, the notches of U-PHAIN-TF and the reference methods do not overlap meaning the results are statistically significant.

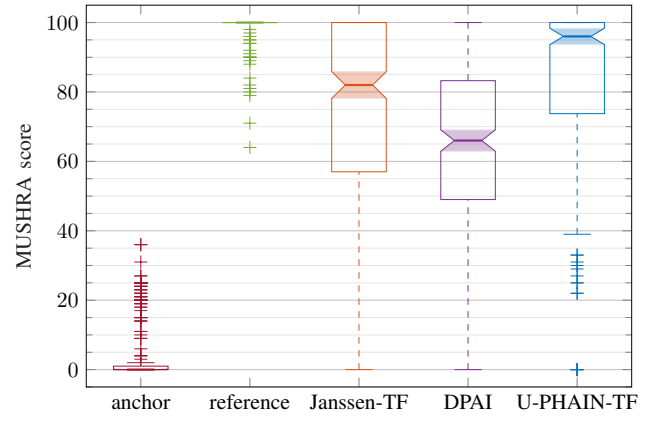


Fig. 9. A boxplot showing the distribution of scores in the listening test. The individual boxes span from the 25th to the 75th percentile of the recorded scores. The notches (filled areas) around the medians (bold lines) are constructed such that boxes whose notches do not overlap have different medians at the 5% statistical significance level.

VII. CONCLUSION

In this paper, we proposed a novel sparsity-based method for spectrogram inpainting, U-PHAIN-TF. Using the phase-aware prior [22], [23], it reduces the energy loss typically seen in sparsity-based approaches. U-PHAIN-TF outperforms recent spectrogram inpainting methods, a deep-prior-based method DPAI and Janssen-TF, which is an autoregression-based method. This conclusion is supported by objective SNR and ODG evaluations and by a MUSHRA-style listening test. Besides its qualitative performance, U-PHAIN-TF is significantly less demanding than the reference methods.

Determining an optimal context window (see Section VI-D) would require a TF-domain adaptation of the method in [21], which does not exist, currently. Future work includes developing such an approach to accelerate the proposed method.

APPENDIX A ALTERNATIVE APPROACH

The problem (14) is not the only possible formulation for spectrogram inpainting that uses a phase-aware prior. The problem can also be written solely in the time-frequency (TF) domain as

$$\underset{\mathbf{X} \in \mathbb{C}^{M \times N}}{\operatorname{argmin}} \lambda \|\mathcal{D}\mathcal{R}_\omega \mathbf{X}\|_1 + \iota_{T_{\text{TF}}}(\mathbf{X}). \quad (25)$$

In contrast to (14), where the primal and dual variables alternate between the time and time-frequency domains, the problem above seeks a solution directly in the time-frequency domain, meaning that no transformation to the time domain is needed. Note that to solve (25), the standard Chambolle–Pock algorithm (CPA) [26] is sufficient, compared with (14). We also formulated an algorithm similar to Alg. 1 for this approach. Then, we compared the objective results of this

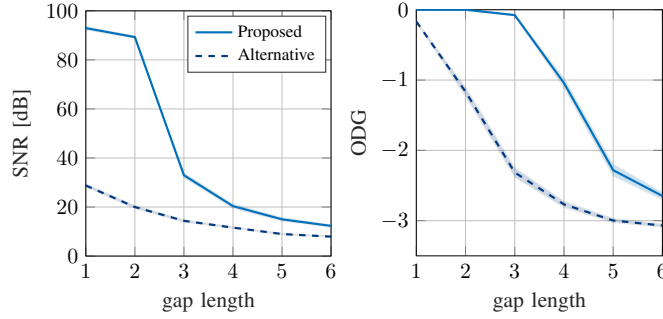


Fig. 10. Comparison on the IRMAS dataset of the proposed method with its alternative version (25) that utilizes solely the TF domain. The mean SNR (left) and ODG (right) are shown.

method with those of the proposed method. The objective metrics were computed on the IRMAS dataset and then averaged. The results comparing these two methods are shown in Fig. 10. The alternative method performs significantly worse in both SNR and ODG. This indicates that reconstruction is more effective when the primal and dual variables of the GCPA alternate between the time and time-frequency domains.

APPENDIX B THRESHOLDING AND NORMS

Similarly to [3], we investigated the performance of the proposed method (U-PHAIN-TF) when the soft thresholding in Alg. 1 is replaced by its alternatives such as p -shrinkage [43] or smooth-hard [43] thresholding. The thresholding operator of p -shrinkage is defined as in [43]

$$\text{shrink}_p(\mathbf{X}) = \text{sgn}(\mathbf{X}) \odot \max(|\mathbf{X}| - \lambda^{2-p}|\mathbf{X}|^{p-1}, 0),$$

where \mathbf{X} is a spectrogram and operations are performed elementwise; λ is a parameter with the same meaning as in (20) and for $p = 1$ this operator coincides with the soft thresholding (20). Similarly, the smooth-hard thresholding operator is defined as

$$\text{SH}(\mathbf{X}) = \mathbf{X} e^{-\alpha/(e^{|\mathbf{X}|-\lambda}-1)^2} \text{ for } |\mathbf{X}| \geq \lambda, \text{ otherwise } 0.$$

As in [43], α is an extra tuning parameter. We then performed several experiments to determine the optimal λ for each thresholding case. We evaluated λ values from 10^{-5} to 10^2 and selected hyperparameters as follows: For p -shrinkage, we chose $p = 0.9$ paired with $\lambda = 0.01$. We explored values of p in $(-1, 1)$. We observed that performance improves as p approaches the soft-thresholding case. For smooth-hard thresholding, we set $\alpha = 10^{-2}$ as in [43] and $\lambda = 10^{-3}$.

Besides modifying the thresholding operators, we also substituted the ℓ_1 -norm with the ℓ_2 -norm and its squared variant (denoted ℓ_2^2). The optimal λ was 1 when using the ℓ_2 -norm and 0.2 when using the ℓ_2^2 -norm.

We then compared all of the above cases with U-PHAIN-TF and its basic variant (denoted B-PHAIN-TF), i.e., the case omitting the instantaneous frequency (IF) update, in terms of both SNR and ODG. In addition, we included an oracle version of B-PHAIN-TF, where the IF is calculated from the ground truth spectrogram (unknown in practice). The ODG

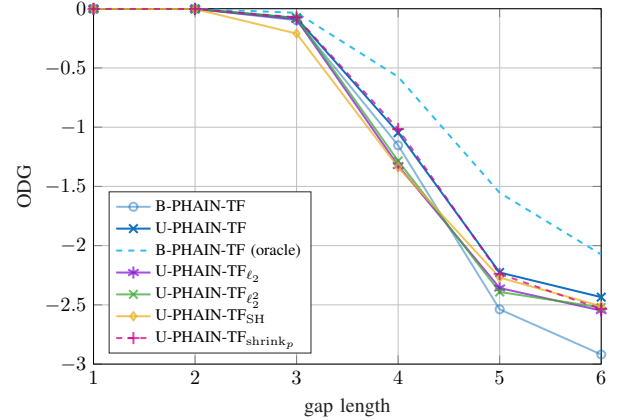


Fig. 11. Comparison on the DPAI dataset of U-PHAIN-TF with different thresholding operators. Only the mean ODG value is shown.

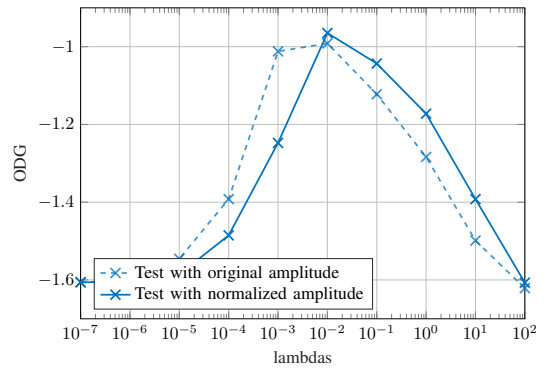


Fig. 12. The normalization test on U-PHAIN-TF. For each amplitude test and lambda value, the ODG metric is calculated for all reconstructions. Only the mean ODG value is shown.

results of this experiment are shown in Fig. 11. We observe that U-PHAIN-TF performs the best when using the ℓ_1 -norm.

APPENDIX C NORMALIZATION

In the paper, we mentioned normalization of the input data for Alg. 1 (i.e., scaling of corrupted spectrogram segments). To assess whether normalization is necessary, we run U-PHAIN-TF under two conditions: with and without normalization. Then, we compare the reconstructions. If the objective results differ, i.e., the optimal lambda value changes in each test, normalization is required. We adopt the following procedure:

- 1) Define a (logarithmically spaced) set of ten values of λ : $\lambda = \{10^{-7}, 10^{-6}, \dots, 10^1, 10^2\}$.
- 2) For each λ , run U-PHAIN-TF on the DPAI dataset and compute the mean ODG results.
- 3) Repeat the previous step; this time normalize the amplitude of each input corrupted spectrogram segment.

The mean ODG values are shown in Fig. 12. The results show that the optimal lambda differs for each test, demonstrating the need for input data normalization. Without normalization, the optimal lambda value would vary for each input.

REFERENCES

[1] A. Adler, V. Emiya, M. G. Jafari, M. Elad, R. Gribonval, and M. D. Plumley, "Audio inpainting," *IEEE Transactions on Audio, Speech, and Language Processing*, vol. 20, no. 3, pp. 922–932, Mar. 2012.

[2] O. Mokrý and P. Rajmic, "Audio inpainting: Revisited and reweighted," *IEEE/ACM Transactions on Audio, Speech, and Language Processing*, vol. 28, pp. 2906–2918, 2020.

[3] T. Tanaka, K. Yatabe, and Y. Oikawa, "PHAIN: Audio inpainting via phase-aware optimization with instantaneous frequency," *IEEE/ACM Transactions on Audio, Speech, and Language Processing*, vol. 32, pp. 4471–4485, 2024.

[4] O. Mokrý, P. Záviška, P. Rajmic, and V. Veselý, "Introducing SPAIN (SParse Audio INpainter)," in *2019 27th European Signal Processing Conference (EUSIPCO)*. IEEE, 2019.

[5] O. Mokrý, P. Magron, T. Oberlin, and C. Févotte, "Algorithms for audio inpainting based on probabilistic nonnegative matrix factorization," *Signal Processing*, p. 10, Dec. 2022. [Online]. Available: <https://www.sciencedirect.com/science/article/pii/S0165168422004443>

[6] I. Toumi and V. Emiya, "Sparse non-local similarity modeling for audio inpainting," in *2018 IEEE International Conference on Acoustics, Speech and Signal Processing (ICASSP)*. IEEE, Apr. 2018.

[7] F. Lieb and H.-G. Stark, "Audio inpainting: Evaluation of time-frequency representations and structured sparsity approaches," *Signal Processing*, vol. 153, pp. 291–299, Dec. 2018.

[8] O. Mokrý and P. Rajmic, "Approximal operator with application to audio inpainting," *Signal Processing*, vol. 179, p. 107807, 2021. [Online]. Available: <http://www.sciencedirect.com/science/article/pii/S0165168420303510>

[9] S. Rajbamshi, G. Tauböck, N. Holighaus, and P. Balazs, "Audio inpainting via ℓ_1 -minimization and dictionary learning," in *2021 29th European Signal Processing Conference (EUSIPCO)*. IEEE, Aug. 2021.

[10] A. J. E. M. Janssen, R. N. J. Veldhuis, and L. B. Vries, "Adaptive interpolation of discrete-time signals that can be modeled as autoregressive processes," *IEEE Trans. Acoustics, Speech and Signal Processing*, vol. 34, no. 2, pp. 317–330, Apr. 1986.

[11] W. Etter, "Restoration of a discrete-time signal segment by interpolation based on the left-sided and right-sided autoregressive parameters," *IEEE Transactions on Signal Processing*, vol. 44, no. 5, pp. 1124–1135, 1996.

[12] Y. Bahat, Y. Y. Schechner, and M. Elad, "Self-content-based audio inpainting," *Signal Processing*, vol. 111, no. 0, pp. 61–72, 2015. [Online]. Available: <http://www.sciencedirect.com/science/article/pii/S0165168414005623>

[13] N. Perraudin, N. Holighaus, P. Majdak, and P. Balazs, "Inpainting of long audio segments with similarity graphs," *IEEE/ACM Transactions on Audio, Speech, and Language Processing*, 2018.

[14] G. Greshler, T. Shaham, and T. Michaeli, "Catch-A-Waveform: Learning to generate audio from a single short example," in *Advances in Neural Information Processing Systems*, M. Ranzato, A. Beygelzimer, Y. Dauphin, P. S. Liang, and J. W. Vaughan, Eds., vol. 34. Curran Associates, Inc., 2021, pp. 20916–20928. [Online]. Available: https://proceedings.neurips.cc/paper_files/paper/2021/file/af21d0c97db2e27e13572cbf59eb343d-Paper.pdf

[15] E. Moliner, J. Lehtinen, and V. Välimäki, "Solving audio inverse problems with a diffusion model," in *2023 IEEE International Conference on Acoustics, Speech and Signal Processing (ICASSP)*. IEEE, Jun. 2023.

[16] M. Bosi and R. Goldberg, *Introduction to Digital Audio Coding and Standards*. Kluwer Academic Publishers, 2003.

[17] A. Marafioti, N. Perraudin, N. Holighaus, and P. Majdak, "A context encoder for audio inpainting," *IEEE/ACM Transactions on Audio, Speech, and Language Processing*, vol. 27, no. 12, pp. 2362–2372, Dec. 2019.

[18] A. Marafioti, P. Majdak, N. Holighaus, and N. Perraudin, "GACELA: A generative adversarial context encoder for long audio inpainting of music," *IEEE Journal of Selected Topics in Signal Processing*, vol. 15, no. 1, pp. 120–131, Jan. 2021.

[19] F. Miotello, M. Pezzoli, L. Comanducci, F. Antonacci, and A. Sarti, "Deep Prior-Based Audio Inpainting Using Multi-Resolution Harmonic Convolutional Neural Networks," *IEEE/ACM Transactions on Audio, Speech, and Language Processing*, pp. 1–11, 2023.

[20] O. Mokrý, P. Balušík, and P. Rajmic, "Janssen 2.0: Audio inpainting in the time-frequency domain," in *2025 33rd European Signal Processing Conference (EUSIPCO)*, 2025, pp. 301–305.

[21] P. Rajmic, H. Bartlová, Z. Průša, and N. Holighaus, "Acceleration of audio inpainting by support restriction," in *2015 7th International Congress on Ultra Modern Telecommunications and Control Systems and Workshops (ICUMT)*. IEEE, Oct. 2015, pp. 325–329.

[22] K. Yatabe and Y. Oikawa, "Phase corrected total variation for audio signals," in *2018 IEEE International Conference on Acoustics, Speech and Signal Processing (ICASSP)*. IEEE, 2018, pp. 656–660.

[23] T. Tanaka, K. Yatabe, and Y. Oikawa, "Phase-aware audio inpainting based on instantaneous frequency," in *2021 Asia-Pacific Signal and Information Processing Association Annual Summit and Conference (APSIPA ASC)*, 2021, pp. 254–258.

[24] O. Mokrý and P. Rajmic, "Tweaking autoregressive methods for inpainting of gaps in audio signals," in *2025 33rd European Signal Processing Conference (EUSIPCO)*, 2025, pp. 311–315.

[25] D. Ulyanov, A. Vedaldi, and V. Lempitsky, "Deep image prior," *International Journal of Computer Vision*, vol. 128, no. 12, 2020. [Online]. Available: <https://doi.org/10.1007/s11263-020-01303-4>

[26] L. Condat, D. Kitahara, A. Contreras, and A. Hirabayashi, "Proximal splitting algorithms for convex optimization: A tour of recent advances, with new twists," *SIAM Review*, vol. 65, no. 2, pp. 375–435, May 2023.

[27] K. Gröchenig, *Foundations of time-frequency analysis*. Birkhäuser, 2001.

[28] Z. Průša, "Stft and dgt phase conventions and phase derivatives interpretation," *Acoustics Research Institute, Austrian Academy of Sciences, Tech. Rep.*, 2015.

[29] K. Yatabe, Y. Masuyama, T. Kusano, and Y. Oikawa, "Representation of complex spectrogram via phase conversion," *Acoustical Science and Technology*, vol. 40, no. 3, pp. 170–177, 2019.

[30] O. Christensen, *Frames and Bases, An Introductory Course*. Boston: Birkhäuser, 2008.

[31] A. Chambolle and T. Pock, "A first-order primal-dual algorithm for convex problems with applications to imaging," *Journal of Mathematical Imaging and Vision*, vol. 40, no. 1, pp. 120–145, 2011.

[32] I. Bayram and M. Kamasak, "A simple prior for audio signals," *IEEE Transactions on Acoustics Speech and Signal Processing*, vol. 21, no. 6, pp. 1190–1200, 2013.

[33] F. Auger and P. Flandrin, "Improving the readability of time-frequency and time-scale representations by the reassignment method," *Signal Processing, IEEE Transactions on*, vol. 43, no. 5, pp. 1068–1089, May 1995.

[34] L. Condat, "A generic proximal algorithm for convex optimization—application to total variation minimization," *Signal Processing Letters, IEEE*, vol. 21, no. 8, pp. 985–989, Aug. 2014.

[35] R. Yamamoto, E. Song, and J.-M. Kim, "Parallel wavegan: A fast waveform generation model based on generative adversarial networks with multi-resolution spectrogram," in *2020 IEEE International Conference on Acoustics, Speech and Signal Processing*. Spain: IEEE, 2020, pp. 6199–6203.

[36] D. P. Kingma and J. Ba, "Adam: A method for stochastic optimization," in *3rd International Conference on Learning Representations, ICLR 2015, San Diego, CA, USA, May 7-9, 2015, Conference Track Proceedings*, Y. Bengio and Y. LeCun, Eds., 2015. [Online]. Available: <http://arxiv.org/abs/1412.6980>

[37] J. J. Bosch, F. Fuhrmann, and P. Herrera, "IRMAS: A dataset for instrument recognition in musical audio signals," 2014. [Online]. Available: 10.5281/ZENODO.1290750

[38] R. Huber and B. Kollmeier, "PEMO-Q—A new method for objective audio quality assessment using a model of auditory perception," *IEEE Trans. Audio Speech Language Proc.*, vol. 14, no. 6, pp. 1902–1911, Nov. 2006.

[39] Z. Průša, P. L. Søndergaard, N. Holighaus, C. Wiesmeyr, and P. Balazs, "The large time-frequency analysis toolbox 2.0," in *Sound, Music, and Motion*, ser. Lecture Notes in Computer Science. Springer International Publishing, 2014, pp. 419–442. [Online]. Available: http://dx.doi.org/10.1007/978-3-319-12976-1_25

[40] T. Kusano, K. Yatabe, and Y. Oikawa, "Window functions with minimum-sidelobe derivatives for computing instantaneous frequency," *IEEE Access*, vol. 10, pp. 32 075–32 092, 2022.

[41] Recommendation ITU-R BS.1534-3: *Method for the subjective assessment of intermediate quality level of audio systems*, International Telecommunication Union Std., Rev. 10/2015, 2015.

[42] M. Schoeffler, S. Bartoschek, F.-R. Stöter, M. Roess, S. Westphal, B. Edler, and J. Herre, "webMUSHRA — A comprehensive framework for web-based listening tests," *Journal of Open Research Software*, vol. 6, no. 1, p. 8, Feb. 2018.

[43] R. Chartrand, "Shrinkage mappings and their induced penalty functions," in *IEEE International Conference on Acoustics, Speech, and Signal Processing*, 2014. [Online]. Available: <http://math.lanl.gov/Research/Publications/Docs/chartrand-2014-shrinkage.pdf>